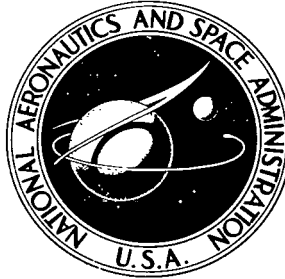


NASA TECHNICAL NOTE



NASA TN D-5908

2.1

NASA TN D-5908

LOAN COPY: RETURN TO
AFWL (WL0L)
KIRTLAND AFB, N MEX



TECH LIBRARY KAFB, NM

EXPERIMENTAL INVESTIGATION OF
HEAT-TRANSFER DISTRIBUTIONS
IN DEEP CAVITIES IN HYPERSONIC
SEPARATED FLOW

by Allan R. Wieting
Langley Research Center
Hampton, Va. 23365



0132742

1. Report No. NASA TN D-5908	2. Government Accession No.	3. Recipient's Catalog No.
4. Title and Subtitle EXPERIMENTAL INVESTIGATION OF HEAT-TRANSFER DISTRIBUTIONS IN DEEP CAVITIES IN HYPERSONIC SEPARATED FLOW		5. Report Date September 1970
7. Author(s) Allan R. Wieting		6. Performing Organization Code
9. Performing Organization Name and Address NASA Langley Research Center Hampton, Va. 23365		8. Performing Organization Report No. L-7059
12. Sponsoring Agency Name and Address National Aeronautics and Space Administration Washington, D.C. 20546		10. Work Unit No. 722-02-10-06
15. Supplementary Notes		11. Contract or Grant No.
16. Abstract <p>An experimental study has been conducted in the 7-inch Mach 7 pilot tunnel at the Langley Research Center to determine the local cold-wall convective heating rates to small rectangular cavities with width-depth ratios varying from 0.063 to 0.524. The tests were conducted at a nominal Mach number of 7.0, zero angle of attack, stagnation temperatures of approximately 3000° R and 3400° R (1700 K and 1900 K), stagnation pressures of approximately 1600 psia and 2000 psia (11 MN/m² and 14 MN/m²), and free-stream unit Reynolds numbers between approximately 1.4 × 10⁶ per foot and 2.3 × 10⁶ per foot (4.6 × 10⁶ per meter and 7.0 × 10⁶ per meter). The results of the study indicate that the local convective heat flux to the cavity increases with cavity width, is a maximum at the top of the forward-facing wall, and decreases monotonically along the wetted perimeter of the cavity. The experimental heat flux distributions are in good agreement with theory when the flow within the cavity is primarily inviscid. The results also indicate that the average cavity heat flux is, in general, less than the corresponding flat-plate heat flux.</p>		13. Type of Report and Period Covered Technical Note
17. Key Words (Suggested by Author(s)) Convective heat transfer Separated flow Cavities	18. Distribution Statement Unclassified - Unlimited	14. Sponsoring Agency Code
19. Security Classif. (of this report) Unclassified	20. Security Classif. (of this page) Unclassified	21. No. of Pages 28
		22. Price* \$3.00

EXPERIMENTAL INVESTIGATION OF HEAT-TRANSFER DISTRIBUTIONS IN DEEP CAVITIES IN HYPERSONIC SEPARATED FLOW

By Allan R. Wieting
Langley Research Center

SUMMARY

An experimental study has been conducted in the 7-inch Mach 7 pilot tunnel at the Langley Research Center to determine the local cold-wall convective heating rates to small rectangular cavities with width-depth ratios varying from 0.063 to 0.524. The tests were conducted at a nominal Mach number of 7.0, zero angle of attack, stagnation temperatures of approximately 3000° R and 3400° R (1700 K and 1900 K), stagnation pressures of approximately 1600 psia and 2000 psia (11 MN/m² and 14 MN/m²), and free-stream unit Reynolds numbers between approximately 1.4×10^6 per foot and 2.3×10^6 per foot (4.6×10^6 per meter and 7.0×10^6 per meter). The results of the study indicate that the local convective heat flux to the cavity increases with cavity width, is a maximum at the top of the forward-facing wall, and decreases monotonically along the wetted perimeter of the cavity. The experimental heat-flux distributions are in good agreement with theory when the flow within the cavity is primarily inviscid. The results also indicate that the average cavity heat flux is, in general, less than the corresponding flat-plate heat flux.

INTRODUCTION

Aerodynamic heating creates a major problem for the designer of hypersonic vehicles because of the resulting high surface temperatures and thermal gradients through the structure. Excessive temperatures and thermal gradients are reflected in structural weight increases to avoid intolerable stress levels or deflections. Hence, to achieve the structural efficiency required for feasible hypersonic flight, the designer must be able to predict the surface heating with a reasonable degree of accuracy. Relationships exist for predicting aerodynamic heating to smooth surfaces. However, many surface defects (gaps at joints, differential ablation, cavities, etc.) exist in any vehicle and are a potential source of boundary-layer separation and possible increased aerodynamic heating.

Separated flow as produced by surface defects has been studied by many investigators. (See refs. 1 to 12.) In 1956 Chapman (ref. 8) produced theoretical results which indicate that the average heating rate to a cavity in laminar separated flow is 56 percent

of that for attached flow. However, his results are applicable only to limited cases (that is, negligible recirculation within the cavity, zero boundary layer at separation point, small viscous shear-layer thickness relative to the cavity dimensions, and so forth). In 1963 Chapman's model was modified by Denison and Baum (ref. 13) to account for a finite boundary layer at the separation point. Their results indicate that the ratio of heat transfer across a free shear layer to that for attached flow varies from 0.61 at the separation point to Chapman's value of 0.56 far downstream. Although the theory agrees, in general, with experimental data (refs. 9 and 10), the local heat-flux distribution along a cavity wall cannot be determined by the theories of reference 8 or reference 13. However, in 1965 Burggraf (ref. 14) analyzed the flow within a rectangular cavity by using an inviscid recirculating core with uniform vorticity and uniform total enthalpy. His analysis permits determination of the heat-flux distribution along the cavity surfaces and the distribution is shown to be in good agreement with experimental data. (See ref. 14.) Most experimental data on separated flow are for cavities with width-depth ratios of 1.0 or greater, whereas the current interest is in "deep" cavities which have width-depth ratios much less than 1.0. This interest is due to the possible application of "open-faced" honeycomb type structures (ref. 11), which would utilize a series of cavities with width-depth ratios less than 1.0, as a means of reducing aerodynamic heating to the primary structure of hypersonic vehicles.

The present paper presents the results of an experimental study conducted in the 7-inch Mach 7 pilot tunnel at the Langley Research Center to determine the local cold-wall convective heating rates to small rectangular cavities with width-depth ratios from 0.063 to 0.524. The tests were conducted at a nominal Mach number of 7, zero angle of attack, stagnation temperatures of approximately 3000° R and 3400° R (1700 K and 1900 K), stagnation pressures of approximately 1600 psia and 2000 psia (11 MN/m² and 14 MN/m²), and at free-stream unit Reynolds numbers between approximately 1.4×10^6 per foot (4.6×10^6 per meter) and 2.3×10^6 per foot (7.0×10^6 per meter). The local convective heat-flux distributions are presented for various cavity widths and are compared with the theory of Burggraf (ref. 14). The average cavity heat flux is determined and compared with the corresponding flat-plate heat flux and the theoretical results of Chapman and Burggraf.

SYMBOLS

The units used for the physical quantities defined in this paper are given both in the U.S. Customary Units and in the International Systems of Units (SI). Factors relating the two systems are given in reference 15 and appendix A.

d	cavity depth, in. (cm)
l	cavity length (transverse to flow), in. (cm)
L	distance from leading edge to separation point, in. (cm)
M	Mach number
N_{Pr}	Prandtl number
$N_{Re,L}$	Reynolds number based on conditions at L
$N_{Re,x}$	unit Reynolds number based on free-stream conditions
n	integer
p	pressure, psia (N/m^2)
Q	normalized heat-flux distribution (eq. (B2))
\dot{Q}	total heating rate, Btu/sec (J/s)
q	local heat flux, Btu/ft ² -sec (W/m^2)
\bar{q}	average heat flux, Btu/ft ² -sec (W/m^2)
r	radius, in. (cm)
s	distance along cavity perimeter measured from $x = 0$, in. (cm)
s_0	wetted perimeter of cavity, in. (cm)
T	temperature, °R (K)
t	time, sec (s)
w	cavity width (streamwise direction), in. (cm)

X	normalized coordinate, $(1 - s/s_0)$
x,y,z	model coordinates (see fig. 1), in. (cm)
δ	boundary-layer thickness
$\zeta(u,v)$	generalized Riemann zeta function

Subscripts:

c	cavity
cr	critical
fp	flat plate
m	model
s	local location
t	total

Superscript:

*	property evaluated at Eckert reference temperature
---	----------------------------------------------------

MODEL, APPARATUS, AND TESTS

Model

A sketch of the basic model configuration is shown in figure 1. The stainless-steel flat-plate holder was $7\frac{3}{4}$ inches (19.7 cm) long and 4 inches (10.2 cm) wide and had a semiwedge-shaped leading edge. The rectangular cavities were formed by slip-cast fused-silica inserts, which also served to insulate the instrumented surfaces from the holder. A 0.012-inch-thick (0.30-mm) stainless-steel plate was attached to the rear and bottom inserts of the cavity to serve as sensing surfaces. These surfaces were instrumented with 20 (36 gage) chromel-alumel thermocouples. Thermocouple locations are given in table I. Forward inserts of various sizes were used to obtain cavity widths w from 0.050 inch to 0.419 inch (0.127 cm to 1.064 cm). The cavity depth d was fixed at 0.8 inch (2.0 cm). The corresponding width-depth ratio w/d varied from 0.063 to

0.524. Scaled profiles of the cavity geometries are presented in figure 1(b). The cavity length (dimension transverse to flow direction) was made large ($l = 3$ inches (7.6 cm)) relative to the cavity width and depth to minimize cavity sidewall effects on the flow at the primary data measurement station, which was at the cavity midlength. To ascertain whether there was significant transverse flow within the cavity which might arise from pressure differences over the cavity length, the cavity length was reduced to 1 inch (2.5 cm) for certain tests. Pertinent cavity details are given in table II.

Static pressures were obtained on the surface of the model and 0.05 inch (0.13 cm) from the bottom surface of the cavity. Pressure orifice locations are given in table III.

A photograph of a typical cavity model test setup is presented in figure 2. As can be seen from the photograph, the leading edge deteriorated during the testing. The maximum nose radius of the cavity holder at the end of testing was approximately 0.06 inch (0.15 cm). The cavities were located far downstream relative to the nose radius and the increased nose bluntness due to its deterioration had no discernible effect on the flow over the cavity proper.

Test Facility

The tests were conducted in the 7-inch Mach 7 pilot tunnel at the Langley Research Center. This tunnel is a hypersonic blowdown facility with a high-energy level obtained by burning a mixture of methane and air under high pressure, the combustion products serving as the test medium to obtain hypersonic flight simulation. A drawing of a section of this tunnel is shown in figure 3. Air is introduced at pressures up to 2300 psia (16 MN/m²), mixed with methane, and then burned in the combustion chamber. The combustion products are then expanded through an axisymmetric contoured nozzle and passed through the free-jet test section. The flow is diffused in a straight-tube diffuser and pumped to the atmosphere by means of a single-stage annular air ejector.

The tunnel operating stagnation-pressure range is approximately 400 psia to 2300 psia (3 MN/m² to 16 MN/m²) and the stagnation temperature range is approximately 1200° R to 3400° R (700 K to 1900 K). Stagnation temperatures and pressures are measured at the downstream end of the combustion chamber just prior to the contraction of the nozzle.

Previous studies (refs. 16 and 17) indicate that the aerodynamic heating and loading coefficients obtained in the combustion products test medium of this facility are comparable with those obtained in air facilities.

Tests

All tests were made at a nominal Mach number of 7 and with the model at an angle of attack of 0° to the flow. Tests were made at stagnation temperatures of approximately

3000° R and 3400° R (1700 K and 1900 K), stagnation pressures of approximately 1600 psia and 2000 psia (11 MN/m² and 14 MN/m²), and at free-stream unit Reynolds numbers between approximately 1.4×10^6 per foot (4.6×10^6 per meter) and 2.3×10^6 per foot (7.0×10^6 per meter). A summary of the test conditions for each cavity is given in table IV. Care was taken to insure that the cavity-sensing surfaces were at room temperature (530° R (294 K)) prior to each test.

The model was held out of the test stream until the test conditions were established and then inserted by means of a hydraulically actuated mechanism. The insertion was accomplished in a time interval of 0.8 second.

The output of model and tunnel thermocouples and transducers was recorded by a steady-state recording system sampling at a rate of 20 frames per second. These data were used to determine tunnel test conditions, cavity surface temperatures, and heating rates. The thermodynamic, transport, and flow properties of the gas used in the reduction of the data were determined by the methods discussed in reference 18.

DATA REDUCTION

Local convective heat fluxes were determined by the transient thin-wall technique. By this technique, the heat-transfer rate is assumed to be equal to the rate at which heat is stored in the surface; thus,

$$q_s = \rho \tau c \frac{dT_s}{dt} \quad (1)$$

where ρ , τ , and c are, respectively, the density, thickness, and specific heat of the sensing surface. The heat-transfer data were determined at the instant the model reached the center line of the test region and before the surface temperature increased enough for radiation and conduction along the sensing surfaces to be significant. In general, the maximum surface temperature rise during this interval was less than 40° R (22 K). Consequently, no correction has been made for surface conduction or radiation in the data presented.

Nicoll (ref. 19) investigated the problems encountered in using the transient "thin wall" technique to determine heat-transfer rates in hypersonic separated flow. The main problem is the time required to establish steady-state flow conditions within the separated region, since the transient thin wall technique is based on the assumption that steady-state conditions exist. Nicoll determined from dimensional analysis that the time required for the establishment of steady-state conditions in a cavity is d^2/ν for diffusion of vorticity and d^2/α for diffusion of heat, where ν is the kinematic viscosity and α is the thermal diffusivity of the test medium. Since for a gas $\alpha = \nu/N_{Pr}$, the times are of the same order, and are approximately 0.2 second for the present test. The

insertion time for the model was approximately 0.8 second; hence, steady-state conditions are believed to exist in the cavity before the model reaches the test region center line.

The accuracy of the data presented is estimated to be within the following limitations:

Pressure, cavity static, p_c	± 0.02 psia (0.14 kN/m ²)
Pressure, model static, p_m	± 0.02 psia (0.14 kN/m ²)
Pressure, stagnation, p_t	± 40 psia (0.28 MN/m ²)
Heat flux, local convective, q	± 0.06 Btu/ft ² -sec (0.68 kW/m ²)
Temperature, stagnation, T_t	$\pm 100^\circ$ R (56 K)

RESULTS AND DISCUSSION

Open cavity flow (that is, the flow bridges the cavity opening) has been found to exist for cavities with w/d ratios up to 14. (See refs. 5 and 20.) Inasmuch as $w/d < 1$ for the present study, the flow is believed to be open cavity flow. Furthermore, it has been shown (refs. 5 and 20) that for this type of cavity flow, the pressure on the bottom surface of the cavity is essentially the same as the pressure on the model surface. Cavity pressure p_c is expressed as a ratio to the model surface pressure p_m and is presented in figure 4 as a function of the cavity width-depth ratio w/d . Data are presented for each cavity length and unit Reynolds number. The ratio p_c/p_m is approximately one for all cases and is apparently independent of Reynolds number and cavity length for the present study. A schematic of the cavity flow considered herein is presented as figure 5.

Heating Distributions

Experimental heat-flux distributions.- Heat-flux distributions along the rear and bottom cavity surfaces are presented in figures 6 to 8 for all cavity configurations and test conditions. In each figure the local heat flux q_s is expressed as a ratio to the corresponding laminar flat-plate heat flux q_{fp} . The value of q_{fp} used for each case is given in table IV and was determined at the cavity midpoint for each test condition from the well-known Pohlhausen relationship for a flat plate (ref. 21) and corrected for compressibility by the Eckert reference temperature method (ref. 22).

The normalized heat-flux distributions along the rear and bottom surface are plotted as a function of the normalized depth x/d and normalized width y/d , respectively. Data from all thermocouple locations are presented. In each case the heat flux is a maximum at $x/d = 0$ (top) and appears to decrease monotonically along the wetted length of the rear and bottom surfaces. The distribution on the rear surface is well represented by a third-order exponential curve fit to the data in a least-squares sense. The effect of unit Reynolds number is indicated in figure 6. Over the small range of unit Reynolds

numbers of the test, there is no discernible Reynolds number effect on the heat-flux ratio. Hence, the local heat flux and flat-plate heat flux increased proportionately with the stream Reynolds number.

Tests with a cavity of 1-inch (2.5-cm) length were made to aid in determining whether any transverse flow effects existed in the 3-inch-long (7.6-cm) cavity. The 1-inch (2.5-cm) length was chosen to minimize any transverse flow effects which might result from pressure differences over the cavity length. Consequently, by comparing the heat-flux distributions in the 1-inch (2.5-cm) cavity with those obtained for the 3-inch (7.6-cm) cavity, the effects of significant transverse flow in the 3-inch (7.6-cm) cavity should be made apparent. The local transverse (z-direction) heat-flux distribution at $x/d = 0.375$ for the 1-inch-long (2.5-cm) cavity ($w/d = 0.211$) is presented in figure 7(a). Inasmuch as there is no discernible variation in the heat flux over the cavity length, it is believed that the flow in this cavity was two dimensional. Heat-flux distributions for the two cavity lengths for a w/d ratio of 0.211 are compared in figure 7(b). The heat-flux distributions for the different length cavities are the same within the scatter of the data. Consequently, any transverse flow effects in the 3-inch (7.6-cm) cavity were small and had a negligible effect on the flow within the cavity. Inasmuch as the external flow over the cavity proper was primarily two-dimensional and no significant transverse flow effects were evident within the cavity, it is believed that the flow inside the 3-inch-long (7.6-cm) cavity was also two-dimensional.

Cavity width effect on the heat-flux distribution is indicated in figure 8. For a given unit Reynolds number, the flat-plate heat flux q_{fp} is essentially constant over the range of cavity sizes; hence, the local heat flux increases with cavity width.

The local heat flux at $x/d = 0$ varies from approximately $0.6q_{fp}$ for the smallest cavity to approximately $1.5q_{fp}$ for the largest cavity. However, in each case, the local heat flux decreases rapidly to less than 10 percent of q_{fp} for $x/d > 0.5$.

Comparison with theory.- The data are compared with the theoretical heat-flux distribution of Burggraf (ref. 14, discussed in appendix B), which is based on a single eddy model (see fig. 5) of an inviscid recirculating core with uniform vorticity and uniform total enthalpy within a rectangular cavity. Application of the theory is limited to cases in which the recirculating cavity flow is primarily inviscid. For the cavity flow to be inviscid and the theory applicable, the test $N_{Re,L}^*$ must be greater than the critical value of $N_{Re,L,cr}^*$ given by equation (B1). If $N_{Re,L}^* < N_{Re,L,cr}^*$, the cavity flow is viscous. The test $N_{Re,L}^*$ for the present study is compared with $N_{Re,L,cr}^*$ in the following table for each cavity:

w/d	$N_{Re,L,cr}^*$	$N_{Re,L}^*$
0.063	2.50×10^5	1.4×10^5
		1.8×10^5
0.211	1.63×10^5	1.4×10^5
		1.8×10^5
0.383	0.45×10^5	1.4×10^5
		1.8×10^5
0.524	0.23×10^5	1.4×10^5
		1.8×10^5

As can be seen from the table, the theory should be valid for the two larger cavities ($w/d = 0.383$ and 0.524) but not valid for the two smaller cavities ($w/d = 0.063$ and 0.211).

The normalized heat-flux distributions q_s/q_{fp} for all cavities are compared with the theory of reference 14 in figures 9 and 10. In these figures the normalized heat-flux ratio q_s/q_{fp} is plotted as a function of the normalized distance X along the wetted perimeter of the cavity. The theoretical curve presented in each figure was determined from equation (B4).

The experimental heat-flux distributions shown in figure 9 are in good agreement with the theory for the cavities with width-depth ratios of 0.383 (fig. 9(a)) and 0.524 (fig. 9(b)). As previously indicated in the table, the theory was indicated to be valid for these two cavities. The heating results from these two cavities indicate that the theory of reference 14 may accurately predict the local heat-flux distributions in rectangular cavities where the cavity flow is inviscid.

As previously discussed, the theory was not expected to yield good results for the cavities with width-depth ratios of 0.063 and 0.211 . A comparison of the experimental heat-flux distribution in these cavities (indicated to have viscous-recirculating flow) and the theoretical heat-flux distribution (ref. 14) is made in figure 10. It appears from the comparison of the theory and the data that for a given size cavity, the local heat flux is larger near the top edge of the rear surface if the recirculating flow within the cavity is primarily viscous. The experimental results of reference 6 show that for a given size cavity, the local and average heat flux to the cavity increases as the external boundary-layer thickness increases. Burggraf (ref. 14) showed that as the external boundary layer thickens, the core within a given cavity becomes proportionately more viscous. Hence, it appears that the results of reference 6 also indicate an increase in cavity heating with a viscous core.

When the cavity core is inviscid (that is, a small boundary layer within the cavity), the energy transport to the cavity comes primarily from the external flow over the cavity, but as the cavity boundary layer thickens and the cavity core becomes viscous, there is additional energy dissipated to the cavity wall as a result of viscous action within the cavity boundary layer. The theoretical results of reference 7 lend credence to this explanation as their results indicate that as the cavity becomes small ($w/d \rightarrow 0$), viscosity and momentum play an equally important role in momentum transfer in the cavity. Consequently, it appears that the heating will be higher to a given cavity if the recirculating cavity flow is viscous rather than inviscid.

Average Cavity Heat Flux

The heat-flux distributions to each surface were integrated over their respective areas and summed to obtain the total heating rate to the cavity surfaces. The experimental heat-flux distributions were used for the rear and bottom surfaces. The heat-flux distribution along the front surface was taken to be that predicted by the theory of Burggraf. The total heating rate to the cavity \dot{Q}_c is compared with the total heating rate to the flat plate (to area wl) \dot{Q}_{fp} as a function of w/d in figure 11. It is apparent from this figure that as w/d approaches zero, the total cavity heating rate approaches the flat-plate value and zero as would be expected. It is also evident that \dot{Q}_c becomes much smaller than \dot{Q}_{fp} as w/d increases. Consequently, it appears that cavities having w/d values greater than about 0.15 receive less heat to their entire surfaces than does a flat plate of area equal to the cavity opening. The ratio of the average cavity heat flux ($\bar{q}_c = \dot{Q}_c/wl$) to the corresponding flat-plate heat flux ($q_{fp} = \dot{Q}_{fp}/wl$) is plotted as a function of the normalized cavity width w/d in figure 12. The experimental heat flux increases from approximately $0.5q_{fp}$ for $w/d = 0.524$ to approximately $1.1q_{fp}$ for $w/d = 0.063$. This trend is due to the nonlinear relationship between the total cavity heating rate and the cavity width w .

The normalized average cavity heat flux as predicted by the theoretical results of references 14 and 8 are also presented in figure 12. Burggraf's equation for the heat-flux distribution (eq. (B2)) is not amenable to normal integration techniques; hence, a graphical technique was used to obtain the results shown.

The theoretical curve indicates that the average cavity heat flux increases slightly as the cavity width decreases. Chapman's theoretical results (ref. 8) indicate that the average cavity heat flux is a function of the Prandtl number only ($\bar{q}_c/q_{fp} = 0.60N_{Pr}^{0.23}$). Inasmuch as the results of reference 14 match Chapman's for $w/d = 0$ (infinitely deep cavity), it is reasonable to assume that Burggraf's result would show the same dependence on the Prandtl number. With this assumption it can be estimated that Burggraf's theoretical results for $N_{Pr} = 1$ overpredict the heat-flux ratio \bar{q}_c/q_{fp} for the present study ($N_{Pr} = 0.75$) by approximately 6 percent.

As noted before, the experimental results are in good agreement with theory for the two larger cavities ($w/d = 0.383$ and $w/d = 0.524$). The average cavity heat flux \bar{q}_c is greater than the theoretical values for the two smaller cavities. However, it is apparent that, in general, the average cavity heat flux is less than the corresponding flat-plate heat flux.

CONCLUDING REMARKS

An experimental study has been conducted in the Langley 7-inch Mach 7 pilot tunnel to determine the local cold-wall convective heating rates to small rectangular cavities with width-depth ratios varying from 0.063 to 0.524. The tests were conducted at a nominal Mach number of 7.0, zero angle of attack, stagnation temperatures of approximately 3000°R and 3400°R (1700 K and 1900 K), stagnation pressures of approximately 1600 psia and 2000 psia (11 MN/m^2 and 14 MN/m^2), and free-stream unit Reynolds numbers between approximately 1.4×10^6 per foot (4.6×10^6 per meter) and 2.3×10^6 per foot (7.0×10^6 per meter).

The results of the present study indicate that the local convective heat flux to the cavity (1) increases as the cavity width is increased, (2) is a maximum at the top of the rear surface, (3) decreases monotonically along the wetted perimeter of the cavity, (4) is less than 10 percent of the corresponding flat-plate heat flux on the bottom surface, (5) is in good agreement with the theory of Burggraf when the flow within the cavity is inviscid, and (6) may be higher than the theoretical value for a given cavity if the recirculating flow is viscous.

The average cavity heat flux is, in general, less than the corresponding flat-plate heat flux for deep cavities with width-depth ratios less than 1.

Langley Research Center,
National Aeronautics and Space Administration,
Hampton, Va., June 23, 1970.

APPENDIX A

CONVERSION OF U.S. CUSTOMARY UNITS TO SI UNITS

Factors required for converting the units used herein to the International System of Units (SI) are given in the following table:

Physical quantity	U.S. Customary Unit	Conversion factor (*)	SI Unit (**)
Heat flux	Btu/ft ² -sec	1.134×10^4	watts/meter ² (W/m ²)
Kinematic viscosity . . .	ft ² /sec	9.290×10^{-2}	meters ² /second (m ² /s)
Length	{ in. per ft	0.0254	meters (m)
		3.28	per meter (m ⁻¹)
Pressure	psi	6.895×10^3	newtons/meter ² (N/m ²)
Temperature	°R	5/9	Kelvin (K)

*Multiply value in U.S. Customary Unit by conversion factor to obtain equivalent value in SI Unit.

**Prefixes to indicate multiples of units are as follows:

Prefix	Multiple
mega (M)	10^6
kilo (k)	10^3
centi (c)	10^{-2}
milli (m)	10^{-3}

APPENDIX B

THEORETICAL HEAT-FLUX DISTRIBUTION

In the analysis of the flow field within rectangular cavities (ref. 14), the flow was visualized as an inviscid rotational core with uniform vorticity and uniform total enthalpy separated from the external flow by a recirculating viscous layer. (See fig. 5.) The equations governing the flow in a square cavity (single recirculating eddy) were determined and then extended by an approximate linearized method to include rectangular cavities. The linearized results were compared in reference 14 with numerical solutions of the full Navier-Stokes equations and were found to be in good agreement.

Application of the analysis of reference 14 is limited to cases for which a central inviscid core flow exists. For cavities with $w < d$, the core becomes completely viscous when the boundary-layer thickness within the cavity δ_c becomes equal to one-half the cavity width w . Hence, the applicability of the theory can be checked by determining the cavity boundary-layer thickness. The critical Reynolds number $N_{Re,L,cr}^*$ at which the flow becomes completely viscous $\delta_c = w/2$ for cavities with $w < d$ is given by (from ref. 14)

$$N_{Re,L,cr}^* = 240 \left(\frac{L}{w} \right)^{4/3} \left(1 + \frac{d}{w} \right) \quad (B1)$$

For the theory to be applicable, $N_{Re,L}^*$ (test Reynolds number) must be greater than $N_{Re,L,cr}$ given by equation (B1).

The linearized analysis of the momentum equations was extended to solve the energy equation which was further simplified by assuming a Prandtl number of one. In reference 14 a normalized heat-flux distribution $Q(X)$ is defined as the ratio of the local heat flux to the surface of a finite-depth cavity to the average heat flux across the separation streamline for an infinitely deep cavity. In the present report the relationship for $Q(X)$ in which total enthalpy and its gradient are matched on the average over the entire separation streamline was used. The equation for the heat-flux distribution is

$$Q(X) = \frac{1}{2\sqrt{2\left(1 + \frac{d}{w}\right)}} \left[\zeta\left(\frac{1}{2}, \frac{s}{2(w+d)}\right) - \zeta\left(\frac{1}{2}, \frac{s+w}{2(w+d)}\right) \right] \quad (B2)$$

where $\zeta(u,v)$ is the generalized Riemann zeta function. The function $\zeta\left(\frac{1}{2}, v\right)$ has been tabulated in reference 23 and is given to an accuracy of one part in 100 000 by the curve fit (from ref. 14)

APPENDIX B

$$\zeta\left(\frac{1}{2}, v\right) = \frac{1}{\sqrt{v}} + \sum_{n=0}^5 a_n (v+1)^n \quad (0 < v < 1) \quad (\text{B3})$$

where the coefficients a_n are

$$\begin{aligned} a_0 &= 0.803323 \\ a_1 &= -3.89728 \\ a_2 &= 2.55002 \\ a_3 &= -1.19121 \\ a_4 &= 0.308284 \\ a_5 &= -0.0335024 \end{aligned}$$

To obtain the local heat flux q_s , it is necessary to multiply $Q(X)$ by the average heat flux across the separation streamline for an infinitely deep cavity. Burggraf reports that for large Reynolds numbers ($Re_L \approx 1/\delta^2$), recirculation is negligible for very deep cavities ($w/d \rightarrow 0$) and concludes that Chapman's model (ref. 8) is a valid representation for an infinitely deep cavity. As a consequence, Burggraf suggests that the normalized heat-flux distribution $Q(X)$ be multiplied by 60 percent of the flat-plate heat flux (Chapman's result for $N_{Pr} = 1$) to obtain the local heat flux to the cavity. Thus, the normalized heat-flux distribution q_s/q_{fp} is given by

$$\frac{q_s}{q_{fp}} = 0.6Q(X) = \frac{0.21}{\sqrt{1 + \frac{d}{w}}} \left[\zeta\left(\frac{1}{2}, \frac{s}{2(w+d)}\right) - \zeta\left(\frac{1}{2}, \frac{s+w}{2(w+d)}\right) \right] \quad (\text{B4})$$

which is used in the text for the comparisons with the experimental data.

REFERENCES

1. Rhudy, J. P.; and Magnan, J. D., Jr.: Investigation of Heat Transfer Distribution in Several Cavity and Step Configurations at Mach 10. AEDC-TDR-64-220, U.S. Air Force, Oct. 1964. (Available from DDC as AD 449 738.)
2. Haugen, R. L.; and Dhanak, A. M.: Momentum Transfer in Turbulent Separated Flow Past a Rectangular Cavity. Trans. ASME, Ser. E: J. Appl. Mech., vol. 33, no. 3, Sept. 1966, pp. 641-646.
3. Nestler, D. E.; Saydah, A. R.; and Auxer, W. L.: Heat Transfer to Steps and Cavities in Hypersonic Turbulent Flow. AIAA Paper No. 68-673, June 1968.
4. Reiman, Thomas C.; and Sabersky, Rolf H.: Laminar Flow Over Rectangular Cavities. Int. J. Heat Mass Transfer (Shorter Commun.), Vol. II, no. 6, June 1968, pp. 1083-1085.
5. Charwat, A. F.; Roos, J. N.; Dewey, F. C., Jr.; and Hitz, J. A.: An Investigation of Separated Flows - Part I: The Pressure Field. J. Aerosp. Sci., vol. 28, no. 6, June 1961, pp. 457-470.
6. Charwat, A. F.; Dewey, C. F., Jr.; Roos, J. N.; and Hitz, J. A.: An Investigation of Separated Flows - Part II: Flow in the Cavity and Heat Transfer. J. Aerospace Sci., vol. 28, no. 7, July 1961, pp. 513-528.
7. Mehta, Unmeel B.; and Lavan, Zalman: Flow in a Two-Dimensional Channel With a Rectangular Cavity. NASA CR-1245, 1969.
8. Chapman, Dean R.: A Theoretical Analysis of Heat Transfer in Regions of Separated Flow. NACA TN 3792, 1956.
9. Larson, Howard K.: Heat Transfer in Separated Flows. J. Aerospace Sci., vol. 26, no. 11, Nov. 1959, pp. 731-738.
10. Nicoll, Kenneth M.: A Study of Laminar Hypersonic Cavity Flows. AIAA J. vol. 2, no. 9, Sept. 1964, pp. 1535-1541.
11. Hunt, L. Roane; and Howell, R. R.: Exploratory Study of Open-Face Honeycomb to Reduce Temperature of Hypersonic Aircraft Structure. NASA TN D-5278, 1969.
12. Hahn, Mansop: Experimental Investigation of Separated Flow Over a Cavity at Hypersonic Speed. AIAA Paper No. 68-672, Amer. Inst. Aeronaut. Astronaut., June 1968.
13. Denison, M. Richard, and Baum, Eric: Compressible Free Shear Layer With Finite Initial Thickness. AIAA J., vol. 1, no. 2, Feb. 1963, pp. 342-349.

14. Burggraf, Odus R.: A Model of Steady Separated Flow in Rectangular Cavities at High Reynolds Number. Proceedings of the 1965 Heat Transfer and Fluid Mechanics Institute, Andrew F. Charwat, ed., Stanford Univ. Press, 1965, pp. 190-229.
15. Comm. on Metric Pract.: ASTM Metric Practice Guide. NBS Handbook 102, U.S. Dept. Com., Mar. 10, 1967.
16. Weinstein, Irving: Heat Transfer and Pressure Distributions on a Hemisphere-Cylinder and a Bluff-Afterbody Model in Methane-Air Combustion Products and in Air. NASA TN D-1503, 1962.
17. Hunt, L. Roane: Aerodynamic Force and Moment Characteristics of Spheres and Cones at Mach 7.0 in Methane-Air Combustion Products. NASA TN D-2801, 1965.
18. Leyhe, E. W., and Howell, R. R.: Calculation Procedure for Thermodynamic, Transport, and Flow Properties of the Combustion Products of a Hydrocarbon Fuel Mixture Burned in Air With Results for Ethylene-Air and Methane-Air Mixtures. NASA TN D-914, 1962.
19. Nicoll, K. M: Use of Transient "Thin-Wall" Technique in Measuring Heat Transfer Rates in Hypersonic Separated Flows. AIAA J., vol. 1, no. 4, Apr. 1963, pp. 940-941.
20. Emery, A. F., Sadunas, J. A., and Loll, M.: Heat Transfer and Pressure Distribution in Open Cavity Flow. Trans. ASME, Ser. C: J. Heat Transfer, vol. 89, no. 1, Feb. 1967, pp. 103-108.
21. Kays, W. M.: Convective Heat and Mass Transfer. McGraw-Hill Book Co., Inc., c.1966.
22. Eckert, Ernst R. G.: Survey on Heat Transfer at High Speeds. ARL 189, U.S. Air Force, Dec. 1961. (Available from DDC as AD 274109.)
23. Powell, E. O.: A Table of the Generalized Riemann Zeta Function in a Particular Case. Quart. J. Mech. App. Math., vol. 5, pt. 1, Mar. 1952, pp. 116-123.

TABLE I.- THERMOCOUPLE LOCATIONS

(a) Rear surface				(b) Bottom surface			
x		z		y		z	
in.	mm	in.	mm	in.	mm	in.	mm
0.01	0.25	0	0	0	0	0	0
.03	.76	-0.25	-6.35	0	0	-0.25	-6.35
.04	1.02	.25	6.35	0	0	-.95	-24.13
.05	1.27	0	0	0.125	3.18	0	0
.10	2.54	0	0	.250	6.35	.125	3.18
.15	3.81	0	0	.375	9.53	0	0
.20	5.08	0	0				
.25	6.35	0	0				
.30	7.62	0	0				
.30	7.62	-.25	-6.35				
.30	7.62	.25	6.35				
.40	10.16	0	0				
.60	15.24	0	0				
.65	16.51	0	0				

TABLE II.- PERTINENT CAVITY DETAILS

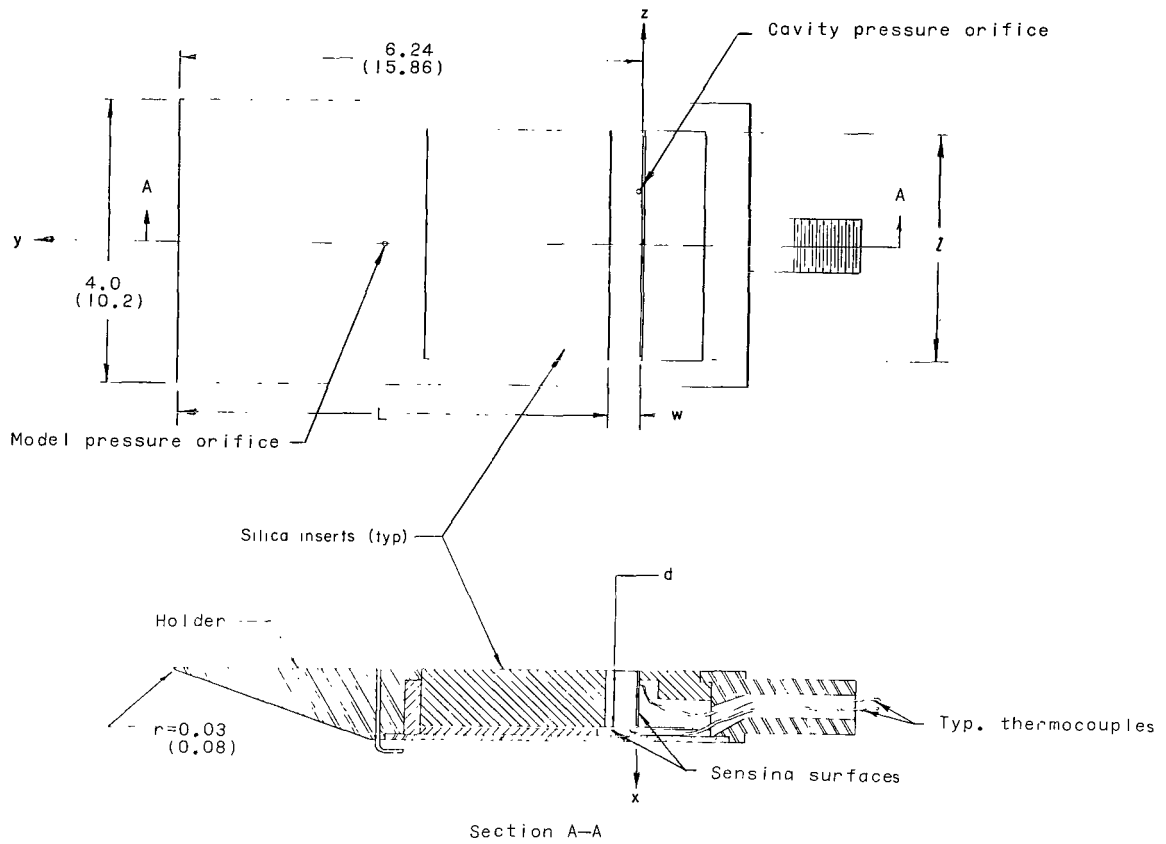
Width, w		Depth, d		Length, l		Width Depth, w/d
in.	cm	in.	cm	in.	cm	
0.050	0.127	0.8	2.0	3	7.6	0.063
0.169	0.429	0.8	2.0	3	7.6	0.211
				1	2.5	
0.306	0.777	0.8	2.0	3	7.6	0.383
				1	2.5	
0.419	1.064	0.8	2.0	3	7.6	0.524

TABLE III.- PRESSURE ORIFICE LOCATIONS

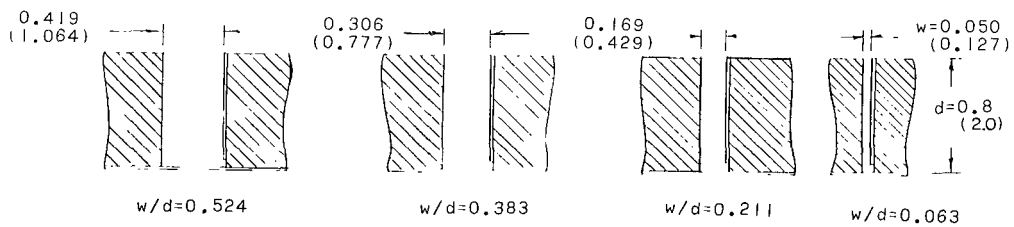
x		y		z	
in.	cm	in.	cm	in.	cm
0	0	3.5	8.9	0	0
.75	1.91	.01	.03	.75	1.91

TABLE IV.- SUMMARY OF TEST CONDITIONS

w/d	l		p _t		T _t		N _{Re,x}		q _{fp}		M
	in.	cm	psia	MN/m ²	°R	K	ft ⁻¹	m ⁻¹	Btu/ft ² -sec	kW/m ²	
0.063	3	7.6	1578	10.9	2950	1639	1.78 × 10 ⁶	5.84 × 10 ⁶	2.58	29.3	6.91
			2092	14.4	2960	1644	2.32 × 10 ⁶	7.61 × 10 ⁶	2.98	33.8	6.94
0.211	3	7.6	1580	10.9	2980	1656	1.73 × 10 ⁶	5.67 × 10 ⁶	2.68	30.4	6.90
			2010	13.9	2960	1644	2.23 × 10 ⁶	7.31 × 10 ⁶	2.96	33.6	6.94
	1	2.5	1588	10.9	3380	1878	1.39 × 10 ⁶	4.56 × 10 ⁶	3.26	37.0	6.78
			2017	13.9	3360	1867	1.76 × 10 ⁶	5.77 × 10 ⁶	3.58	40.6	6.78
0.383	3	7.6	1590	11.0	2970	1650	1.74 × 10 ⁶	5.71 × 10 ⁶	2.68	30.4	6.90
			2005	13.8	2960	1644	2.27 × 10 ⁶	7.45 × 10 ⁶	3.01	34.1	6.94
	1	2.5	1590	11.0	3380	1878	1.38 × 10 ⁶	4.53 × 10 ⁶	3.29	37.3	6.78
			2018	13.9	3350	1861	1.75 × 10 ⁶	5.74 × 10 ⁶	3.62	41.1	6.78
0.524	3	7.6	1576	10.9	2970	1650	1.73 × 10 ⁶	5.67 × 10 ⁶	2.71	30.7	6.90
			2010	13.9	2920	1622	2.25 × 10 ⁶	7.38 × 10 ⁶	2.94	33.3	6.90



(a) Model assembly.



(b) Scaled cavity profiles.

Figure 1.- Sketch of basic model configuration and cavity profiles.
 (All dimensions are given first in inches and parenthetically
 in centimeters.)

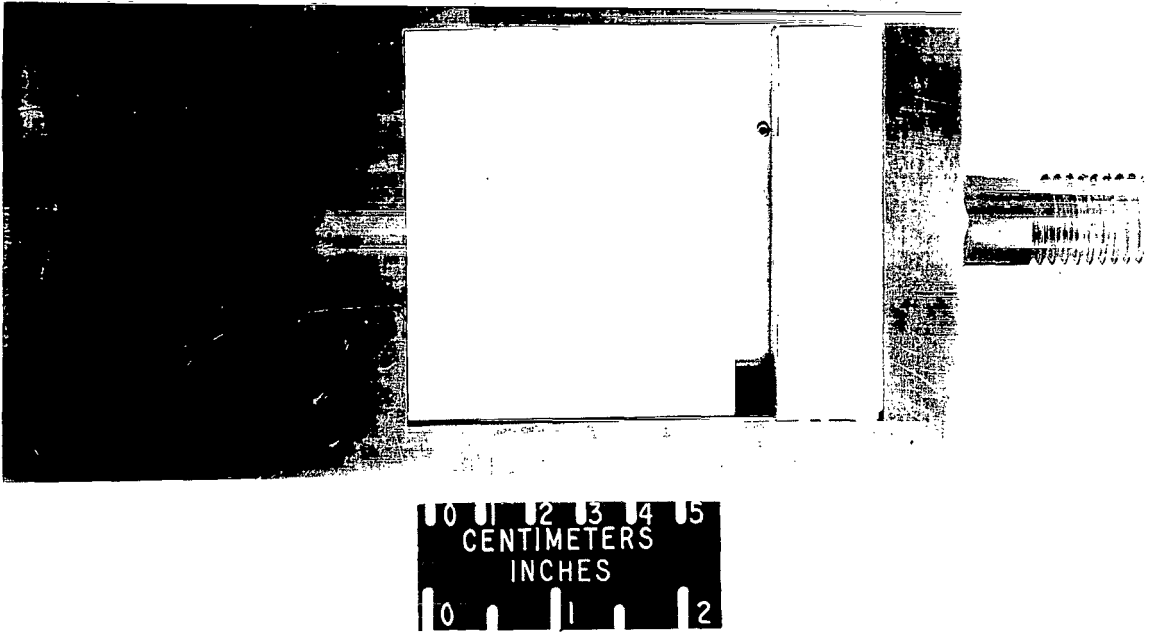


Figure 2.- Photograph of typical model test setup. $w/d = 0.383$. L-70-4704

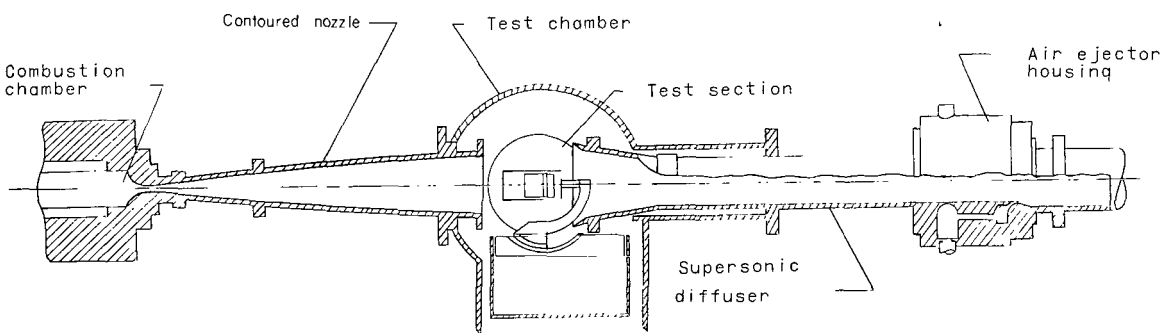


Figure 3.- Schematic of 7-inch Mach 7 pilot tunnel at the Langley Research Center.

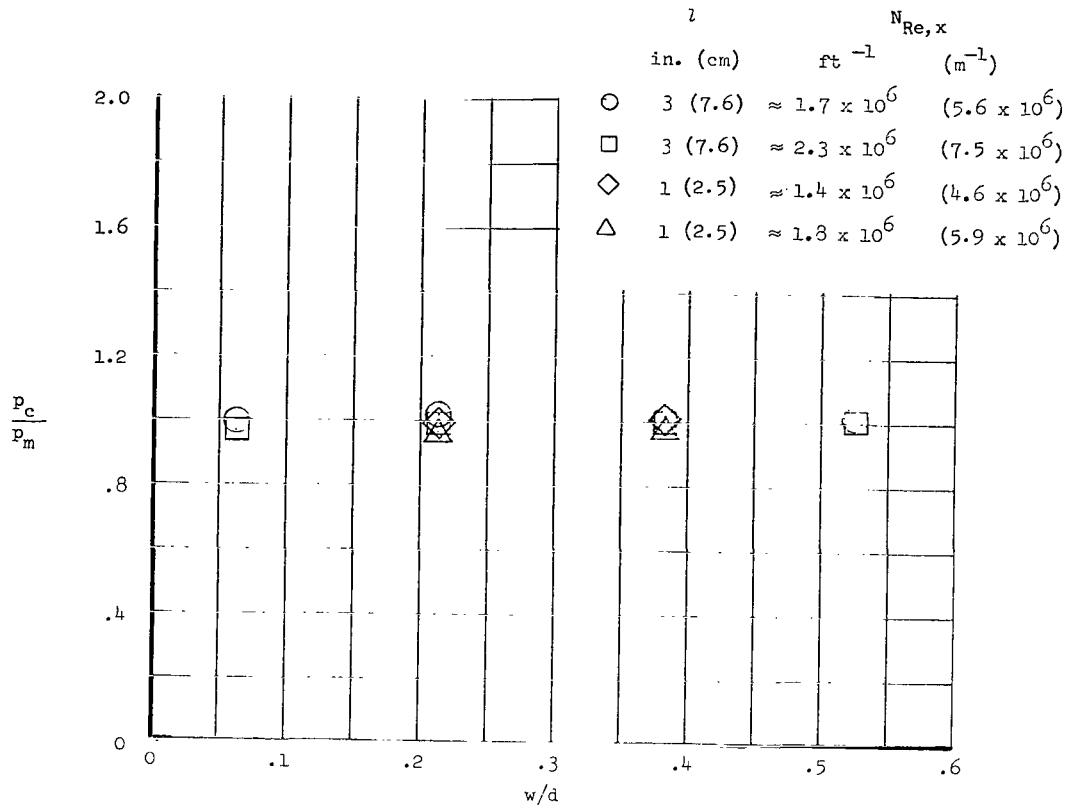


Figure 4.- Ratio of cavity pressure to model surface pressure.

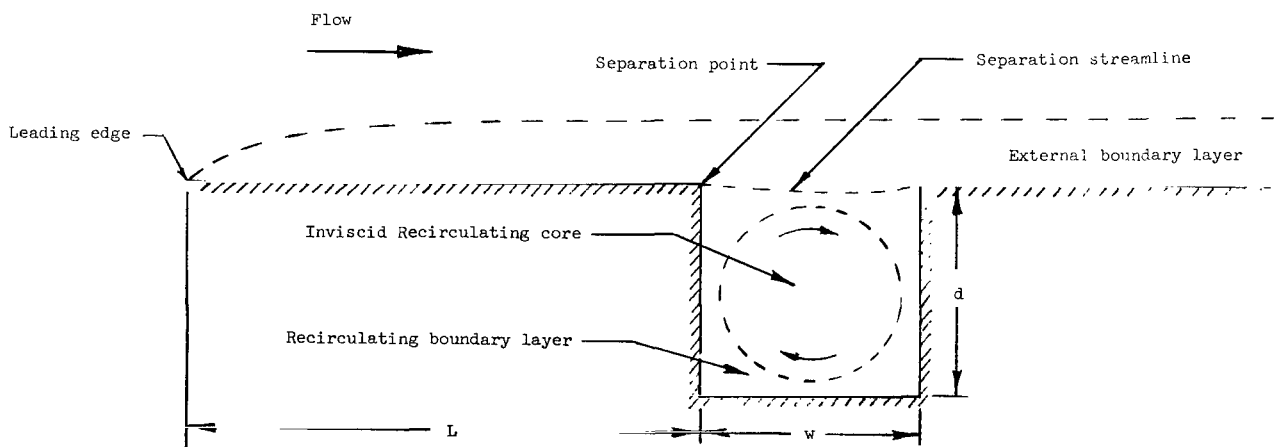
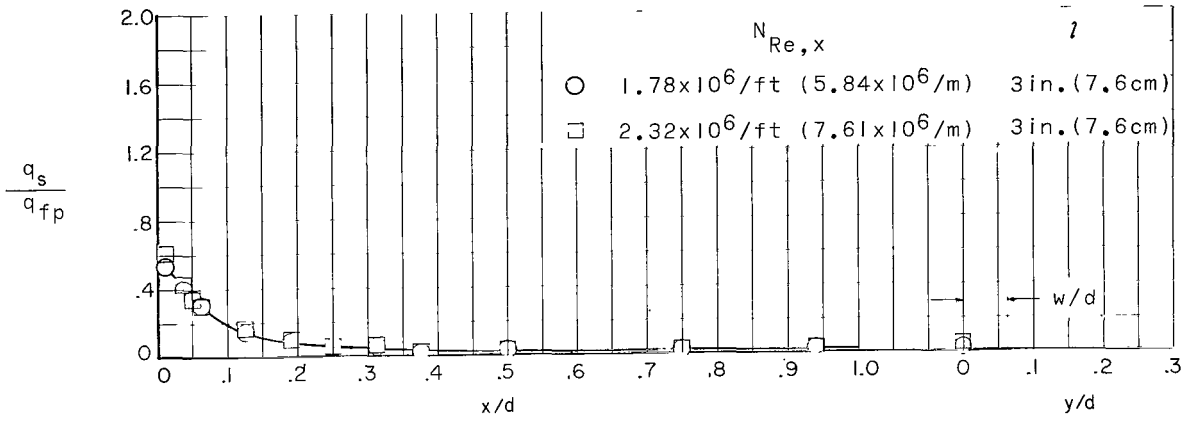
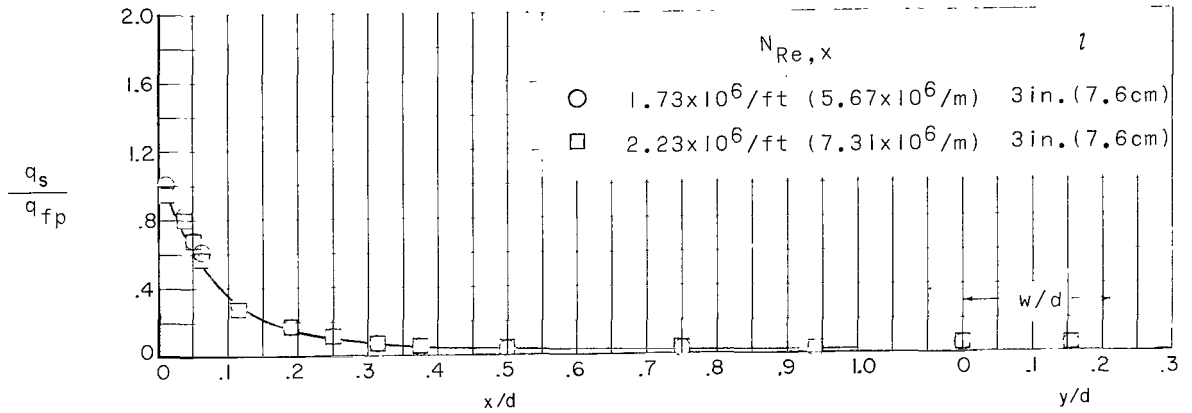


Figure 5.- Schematic of cavity flow.

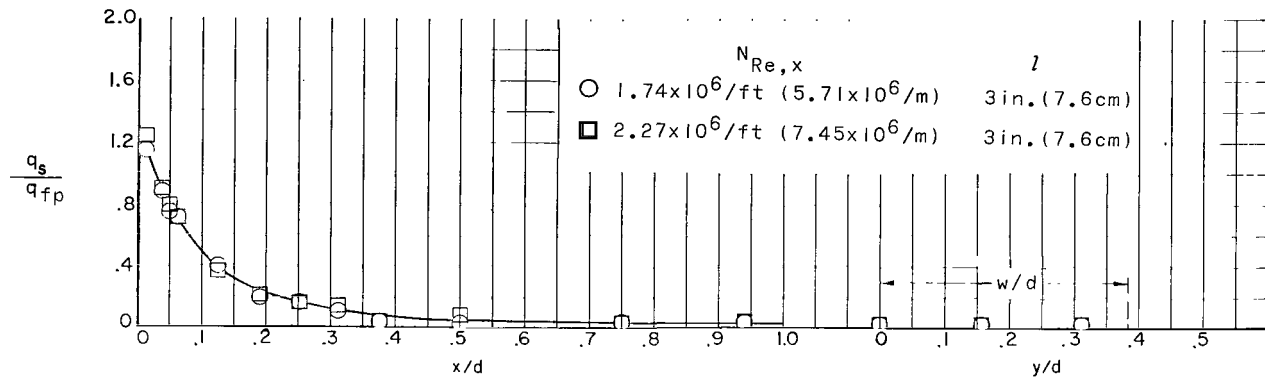


(a) $w/d = 0.063$.

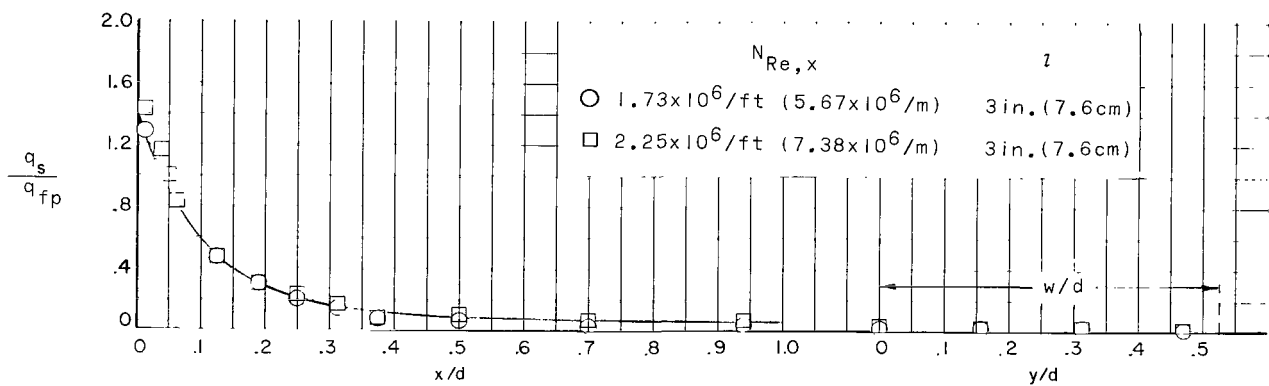


(b) $w/d = 0.211$.

Figure 6.- Normalized heat-flux distributions on cavity rear and bottom surfaces.

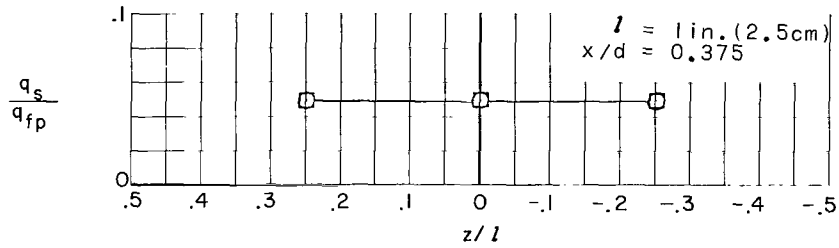


(c) $w/d = 0.383$.

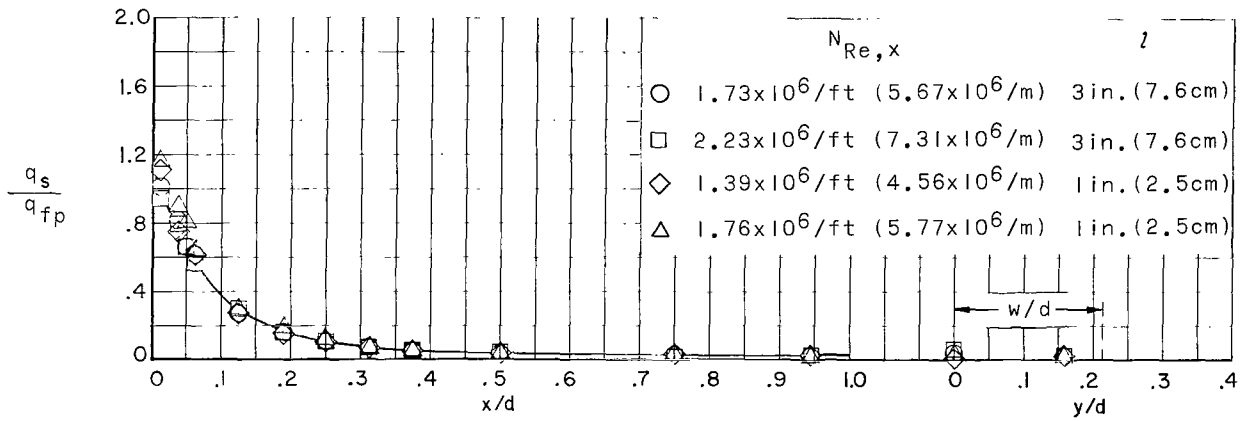


(d) $w/d = 0.524$.

Figure 6.- Concluded.



(a) Transverse heat-flux variation.



(b) Comparison of heat-flux distributions along cavity perimeter.

Figure 7.- Effect of cavity length on cavity heat-flux distribution. $w/d = 0.21$.

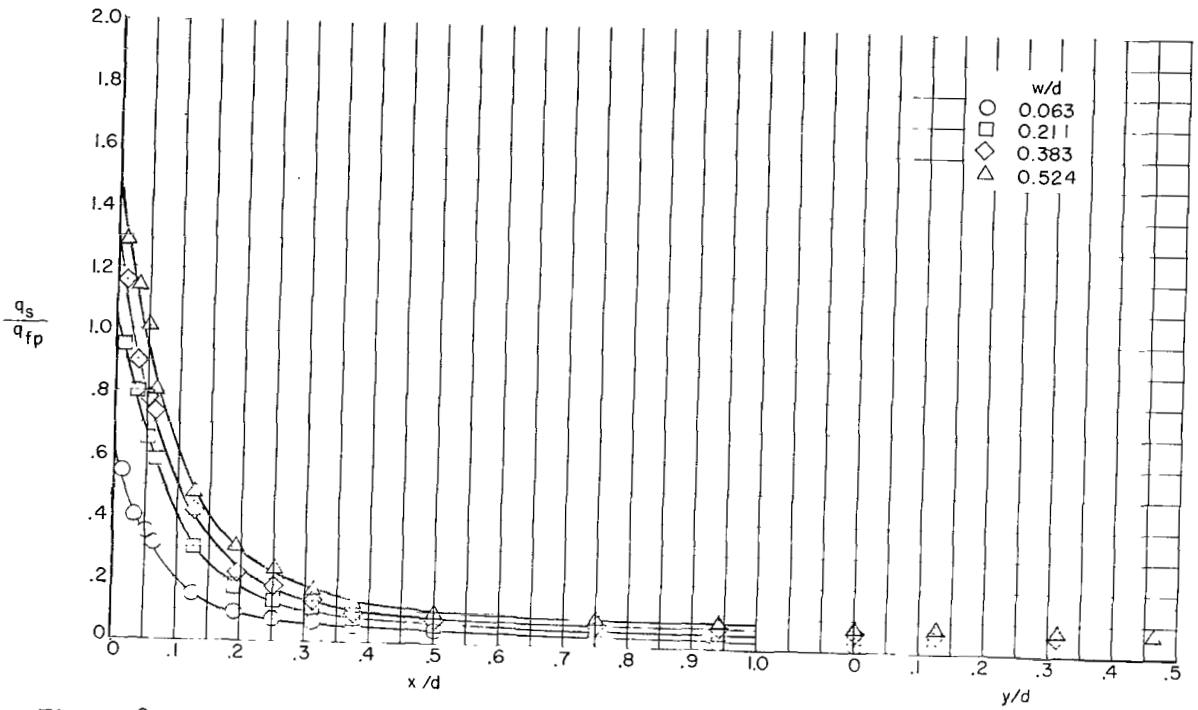
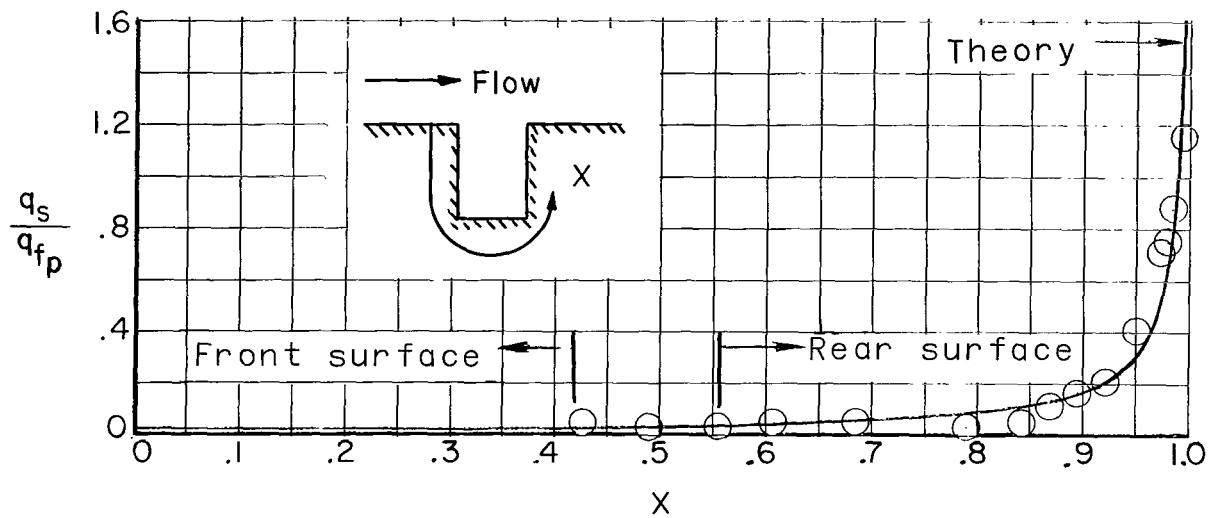
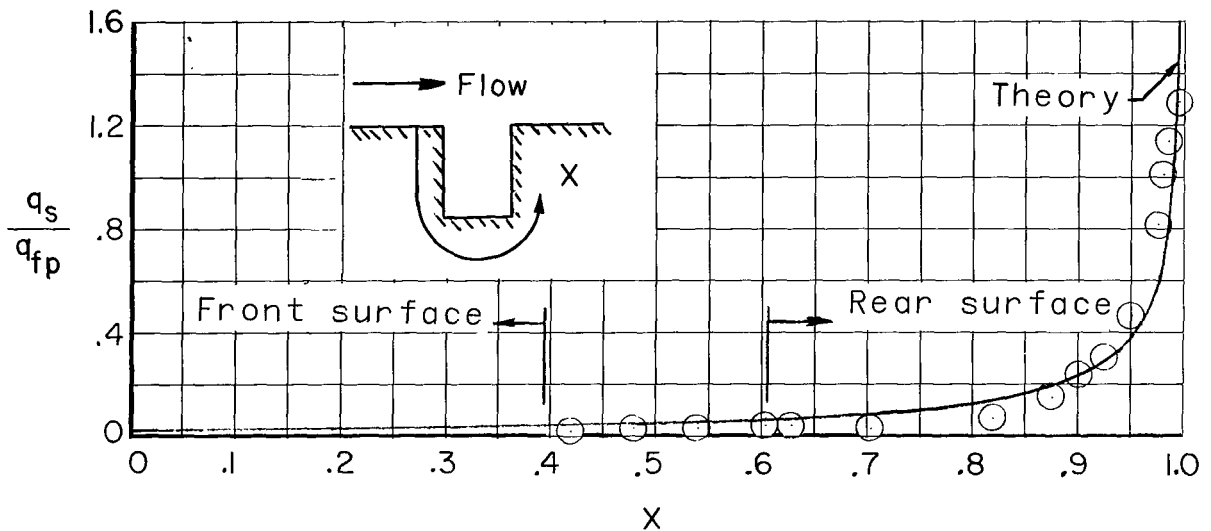


Figure 8.- Effect of cavity width-depth ratio on cavity heat-flux distribution.
 $N_{Re,x} \approx 1.7 \times 10^6/\text{ft}$ ($5.6 \times 10^6/\text{m}$); $l = 3$ inches (7.6 cm).

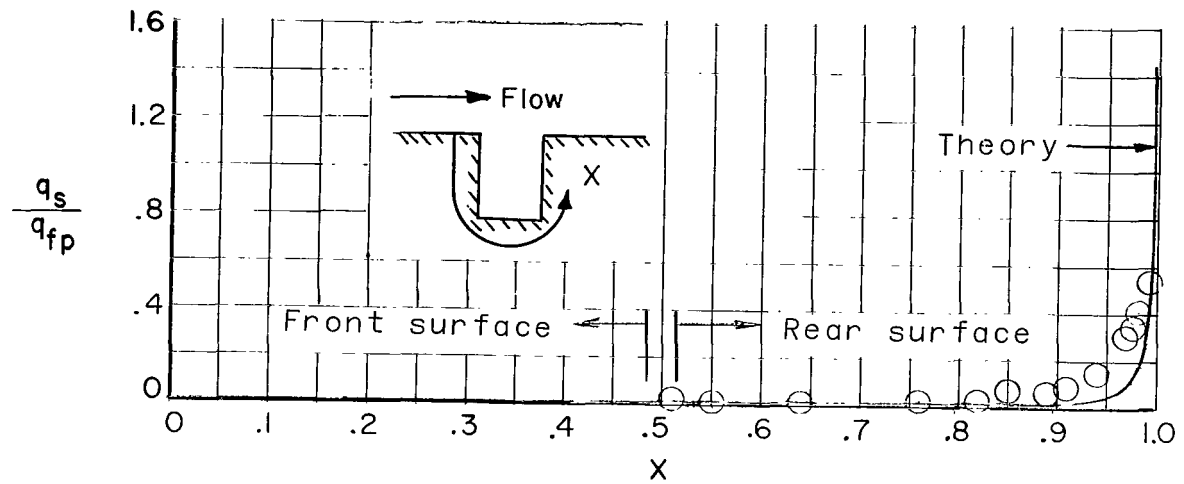


(a) $w/d = 0.383$.

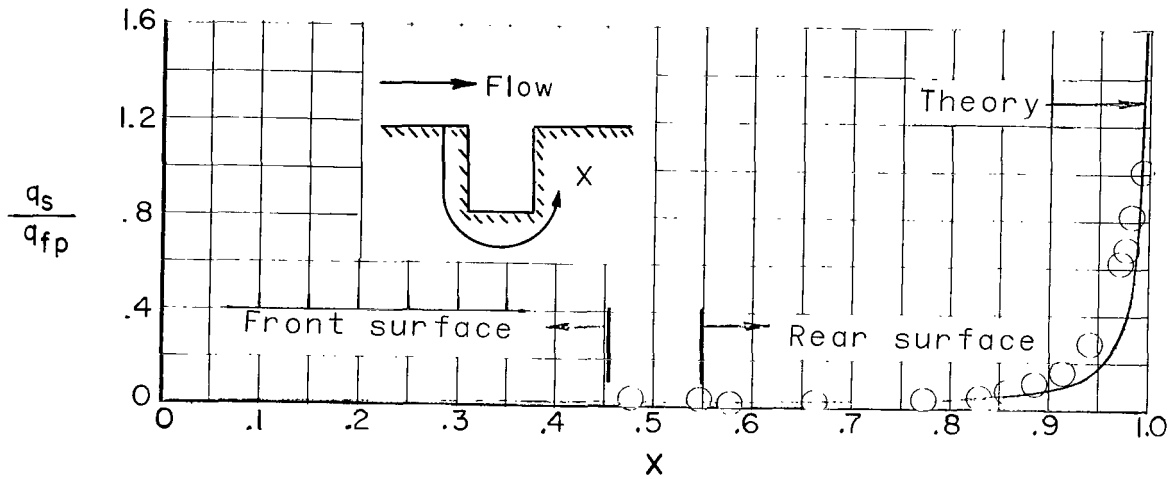


(b) $w/d = 0.524$.

Figure 9.- Comparison of experimental heat-flux distribution in a cavity with an inviscid core with the theory of reference 14. $N_{Re,x} \approx 1.7 \times 10^6/ft$ ($5.6 \times 10^6/m$).



(a) $w/d = 0.063$.



(b) $w/d = 0.211$.

Figure 10.- Comparison of experimental heat-flux distribution in a cavity with a viscous core with the theory of reference 14. $N_{Re,x} \approx 1.7 \times 10^6/lb$ ($5.6 \times 10^6/m$).

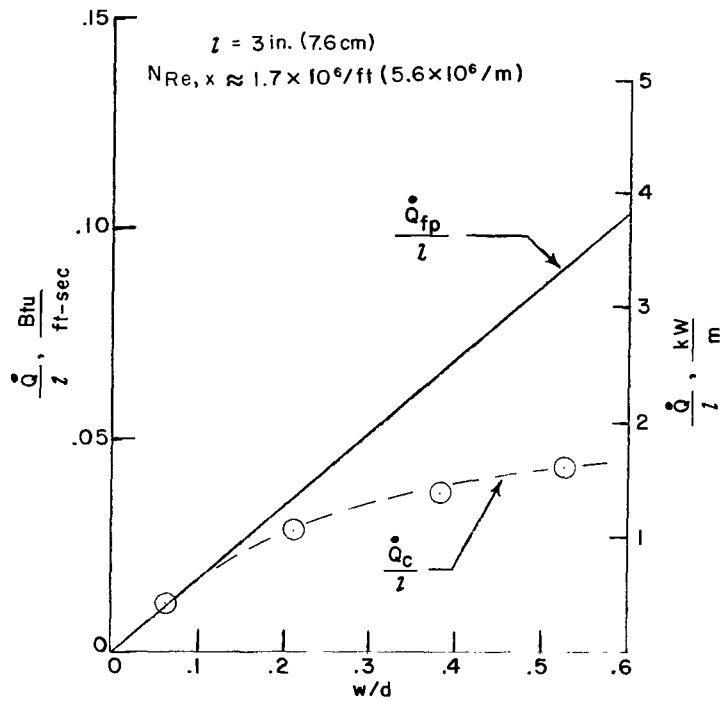


Figure 11.- Comparison of total cavity heating rate and total flat-plate heating rate. (d = 0.8 inch (2.0 cm).)

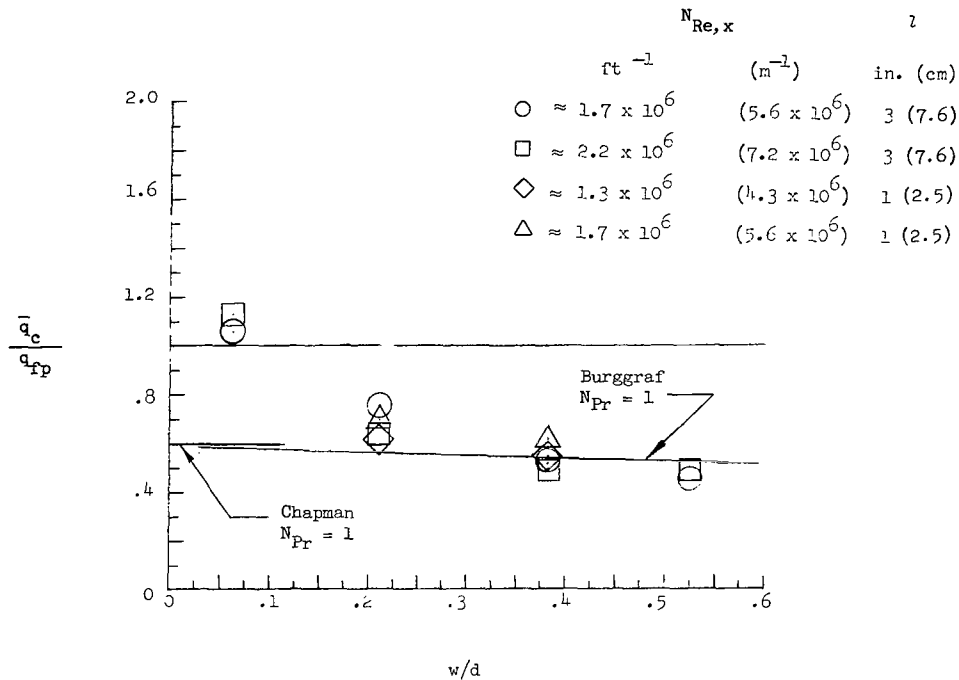


Figure 12.- Ratio of average cavity heat flux to flat-plate heat flux.

NATIONAL AERONAUTICS AND SPACE ADMINISTRATION
WASHINGTON, D. C. 20546
OFFICIAL BUSINESS

FIRST CLASS MAIL



POSTAGE AND FEES PAID
NATIONAL AERONAUTICS AND
SPACE ADMINISTRATION

01U 001 26 51 3DS 70240 00903
AIR FORCE WEAPONS LABORATORY /WL0L/
KIRTLAND AFB, NEW MEXICO 87117

ATT E. LOU BOWMAN, CHIEF, TECH. LIBRARY

POSTMASTER: If Undeliverable (Section 158
Postal Manual) Do Not Return

"The aeronautical and space activities of the United States shall be conducted so as to contribute . . . to the expansion of human knowledge of phenomena in the atmosphere and space. The Administration shall provide for the widest practicable and appropriate dissemination of information concerning its activities and the results thereof."

— NATIONAL AERONAUTICS AND SPACE ACT OF 1958

NASA SCIENTIFIC AND TECHNICAL PUBLICATIONS

TECHNICAL REPORTS: Scientific and technical information considered important, complete, and a lasting contribution to existing knowledge.

TECHNICAL NOTES: Information less broad in scope but nevertheless of importance as a contribution to existing knowledge.

TECHNICAL MEMORANDUMS: Information receiving limited distribution because of preliminary data, security classification, or other reasons.

CONTRACTOR REPORTS: Scientific and technical information generated under a NASA contract or grant and considered an important contribution to existing knowledge.

TECHNICAL TRANSLATIONS: Information published in a foreign language considered to merit NASA distribution in English.

SPECIAL PUBLICATIONS: Information derived from or of value to NASA activities. Publications include conference proceedings, monographs, data compilations, handbooks, sourcebooks, and special bibliographies.

TECHNOLOGY UTILIZATION PUBLICATIONS: Information on technology used by NASA that may be of particular interest in commercial and other non-aerospace applications. Publications include Tech Briefs, Technology Utilization Reports and Notes, and Technology Surveys.

Details on the availability of these publications may be obtained from:

SCIENTIFIC AND TECHNICAL INFORMATION DIVISION
NATIONAL AERONAUTICS AND SPACE ADMINISTRATION
Washington, D.C. 20546